Noname manuscript No.
(will be inserted by the editor)

Optimization of the ligating additives mixing technology during the a Rheinsahl-Heraeus (RH) process by CFD methods

Moschenko G. Maksim · Elena A. Sudorgina · Anastasija J. Cumika · Michail P. Gusev

Received: date / Accepted: date

Abstract Ferrosilicon and aluminum additives mixing during the Rheinsahl-Heraeus (RH) process was investigated by means of CFD numerical simulation. The main goal of the research was finding the optimal mixing parameters to minimize the mixing time to decrease the amount of carbon pick up in molten steel. A simple but robust CFD model of the mixing process in the RH degasser was developed in Ansys CFX software. Results were validated with the experiments performed on the industrial plant. The results of the simulation have shown that the steel flow velocity in the down snorkel has the greatest influence in the mixing time. While snorkel immersion depth has only a slight effect on the mixing time. Research results from the numerical model were implemented in the industrial RH degasser. Optimized mixing time resulted in the decrease of carbon pick by 7 ppm and the steel grade was improved.

Keywords RH degasser · Rheinsahl-Heraeus · optimal mixing time of additives · additives mixing · numerical simulation · CFD · optimization · electrical steel · ultralow-carbon steel

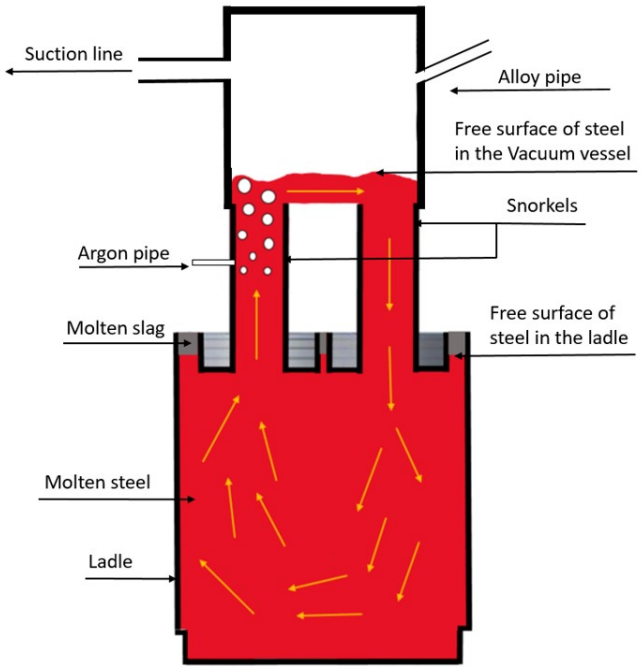

Fig. 1 The scheme of RH degassing process [7]

1 Introduction

The Rheinsahl-Heraeus (RH) process as a type of secondary refining technique is mainly used for the removal of dissolved C from molten steel in ultra-low carbon steel manufacturing [1]. Besides carbon reduction in steel, RH also plays an important role in degassing, desulfurization, inclusion removal [2,3,4,5] and homogenizing the temperature and alloys additives that are added to the steel during the RH process. Besides, RH process is also recommended for silicon electrical steel producing [6]. The molten steel is circulated between the vacuum chamber and ladle due to the effect of argon injected through snorkel nozzles under vacuum conditions. A vacuum is injected in the upper chamber, which raises the melt through the nozzles into the chamber to a certain level. The metal level in the chamber is determined by the density of the metal, gravity, and

M. Moschenko · E. Sudorogina
NLMK, Ulitsa Bol'shaya Ordynka, 40, bld.3, Moscow, 119017
Tel.: +7-968-963-23-85
E-mail: moschenko_mg@nlmk.com

A. Cumika · M. Gusev
Skolkovo Institute of Science and Technology, Bol'shoy Bul'var, 30, Moscow, Moscow Oblast, 143026

the difference between atmospheric pressure and chamber pressure. The melt circulates between the vacuum chamber and the ladle due to the injected argon gas bubbles in one of the snorkels. Bubbles of lift gas rise upward, bringing liquid metal with them. A portion of the newly flowing metal into the chamber displaces the metal in the chamber that flows through the downstream pipe, maintaining the circulation process.

During the silicon electrical steel production, the RH process can be divided into two consecutive steps: decarbonization and alloying. First, the target de-C level is reached, and then alloying additives are introduced. Ferrosilicon, as a source of silicon, in the amount of 3% and aluminum in the amount of 1% are used as alloying additives. At the same time, an increase in the carbon content while mixing is experimentally observed. The longer the mixing process, the higher the level of carbon pick-up.

It is known that when alloying additions are introduced, an increase in carbon in steel is observed. This undesirable effect can be caused by the transfer of carbon from the ladle refractory material into the melt. This process is observed due to the fact that some of the added Si and Al pass into the slag in the form of oxides, increasing the solubility of the MgO-C lining in the slag [8,9,11]. From laboratory experiments it was observed that the destruction of refractories linearly increases with time. In this case, the corrosion rate increases with an increase in the metal speed relative to the refractory [12,13].

Considering the impossibility to replace or reduce the additives, carbon pick-up during the mixing can be reduced by:

1. selecting the appropriate slag / refractory pair [14,15].
2. optimization of the refractory material [16,17,18].
3. selecting the mixing mode, when alloying additives are homogeneously distributed in the steel melt, and the carbon content remains at an acceptably low level.

The first and second methods are economically and technologically difficult to implement, so it would be desirable to establish optimal mixing parameters for the distribution of alloying additives.

Mixing in RH degasser has been studied for a long time, and there are both physical and numerical models created throughout the years. Among numerical models, there exist different single-phase [19,20,21,22,23,24,25] studies as well as models for the multiphase studies. Algebraic slip mixture model (ASM) [26,27] is a simplified multiphase model where gas and liquid phases are treated as one mixture phase; however, different phases move at different velocities. There are models, such as the Euler-Euler [5,28,29,30] model and Euler-Lagrange [30] model, with the improvement from VOF-DPM [7,31,32,33,34] coupled model. These models consider argon bubbles as a separate phase. In the volume of fluid (VOF) method, the steel is considered as a continuous phase, and gas bubbles are tracked using the discrete phase model (DPM). G.Chen, S.He, and Y.Li [31] made a more complicated and precise VOF-DPM (Volume of Fluid - Discrete Phase Model) model by looking at the expansion of the argon bubbles. VOF-DPM model considered the most precise method, and Yu Liu et al. [35] made a superb study on comparing Euler – Euler approach with the Euler – Lagrange approach for the mixing model in the ladle with the gas injection to prove the advantage of the Euler-Lagrange with VOF-DPM model. These models were implemented in various solvers such as Ansys Fluent [31,33,34,36], Ansys CFX [5,26,27,30,37], and in earlier works Phoenics [20,29].

On the experimental side, there were performed numerous water model trials, where water RH prototypes are based on the real RH degassers usually scaled to a smaller size. To track the homogeneity of the fluid NaCl [19,30,38,39,40,41,42] and KCl [26,33,43,44,45,46,47] were used as a tracer, and the conductivity between two points was measured. From the conductivity measurements, one can get data for the mixing time. To observe the flow patterns, scientists used colorants such as $KMnO_4$ ink tracers [30,40,47,48,49]. For flow velocity measurements, Ultrasonic flow meter [28,44], Particle Image Velocimetry (PIV) [42,43,47], or CCD camera [23] were used.

Computer simulations are much cheaper and more applicable for finding optimum parameters, but they need physical validation. Some researchers [19,26,28,30,33,49] performed both water and numerical models where the physical model was a validation for their flexible mathematical model. However, not many researchers performed industrial experiments. Kuwabara et al. [50] did considerable experimental research on the real plant to study the decarburization behavior during the RH process under various conditions. Other researchers [20,23,30,34,43] mentioned in their work that they took some steel samples during the RH process to validate their water or numerical models. However, researchers focused more on the mathematical models than the experimental part of their research.

Among performed research, several main parameters were found to affect mixing time, and these parameters gained most of the interest from the scientists. Operating parameters such as snorkel immersion depth (SID) [19,20,22,32,36,38,39,42,49], and argon gas blowing rate [21,22,24,29,30,31,32,38,39,40,42,45,48,49] are most popular as well as they have the most influence on the cir-

culation rate and mixing time. Other operational parameters that researchers have studied include vacuum pressure [22,39,44], atmospheric pressure [32], and argon gas blowing angle [48]. Despite the easiness of varying operating parameters, scientists conducted researches on how non-operational parameters affect the mixing time and circulation rate. Varying the number of nozzles [22,33,41,43,44] is most common in research and industry, as well as it is proved to be an efficient parameter. Also, varying the diameters of the snorkels [20,22,24,36,44,46], and nozzles [44,45], along with increasing the number of nozzles, is an effective method to decrease mixing time. Researchers also studied setups with bottom gas blowing [5,7,27] the multiple numbers of snorkels [21,36], and oval snorkels [43,50]. Besides, B.Li and F. Tsukihashi [28], and D-Q.Geng, H.Lei, and J-C.He [37] studied how traveling magnetic field around the snorkels affects the circulation flow.

It should be noted that SID increase not always shows an increase in mixing time [38,42]. The reason for that might be the dead zones where the mixing is happening at the latest. These zones are usually near the free surface to the sides and between the snorkels. Therefore, by not looking at the dead zone areas, one might not see that after some time, the fluid is still not homogeneous. B.Zhu et al. [30] and D.Niu et al. [49] did a study to show the dead zones that appear in the RH degasser.

The purpose of this research is not covered in the precise numerical simulation modeling of the RH degasser, as in the works discussed above. In this paper, the efforts were focused on developing a reliable and predictable numerical model that could show the dependency of time required for chemical homogenization and operational parameters of RH degasser. After, the results of the research are planned to be used for the industrial RH degasser operation. Summarizing what has been written above, the purpose of the research is the following:

1. Develop the most simplified but predictable CFD model for an estimation of the minimum required time period for the homogenization of dropped additive alloying.
2. Verify and validate the model as well as investigate the influence of variation parameter (SID, circulation rate).
3. Implement minimum required mixing time and evaluate the influence of mixing time on carbon pick-up.

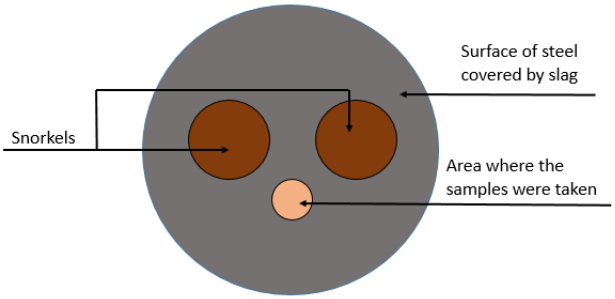

Fig. 2 Position of the region where the samples were taken (ladle, top view)

2 Motivation

That is a common practice to take a probes after decarburization process and after the mixing of alloying materials. Probes are taken form the upper layer of molten steel, making a hole in a slag. Sampler is plunged in molten steel on 200-400 mm below free surface. The top view of region of taking a probe is shown in the Figure 2. Samplers Heraeus Electro-Nite Samp-O-Line without Zr for low carbon steel are used. Comparison of two probes of the same heat usually detects a picking-up of carbon. Carbon amount has been measured with optical atom emission spectrometer ARL ISPARK 8860.

Based on the experimental data, a hypothesis was formulated that the increase in carbon depends on the content of Si and Al, the time of mixing the additives with the corresponding components, and the number of heats carried out in the ladle before the considered melting. It would be more accurate to use data on the content of $Al2O_3$ and SiO_2 in the slag, but such information is not available for all the heats. The analysis assumes that there is a correlation between the element content in the steel and the corresponding oxide content in the slag. It was assumed that there is a carbonization function f represented by the equation [1].

$$f = \left[a\left(Al * t_{Al}\right)^b + c\left(Si * t_{Si}\right)^d\right] * raf^e \quad [1]$$

where Al and Si are aluminum and silicon concentration measured after mixing time, t_{Al} and t_{Si} – duration of mixing of Al and ferrosilicon alloy; raf - he number of heats for a ladle after the last repair; a, b, c, d, e - coefficients. By solving the optimization problem through maximizing the correlation coefficient between f and carbon gain, the coefficients a, b, c, d, e were determined. The function f do not depend on the stirring rate, because for all heats in this study, homogenization was performed at the maximum possible Ar consumption.

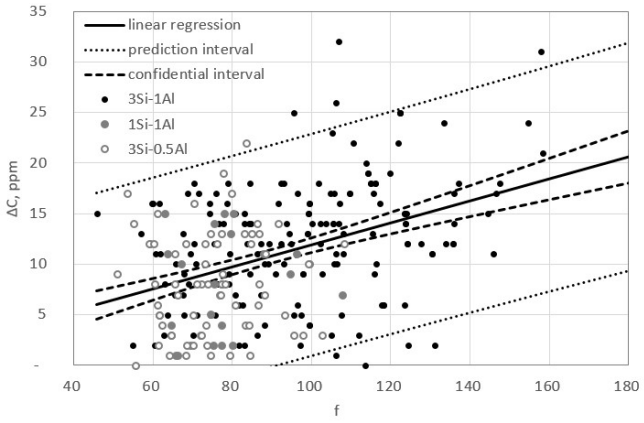

Fig. 3 Dependence of carbon increase at ACV ΔC from the carburization function f, for 2018-2020 years data for various IETS brands

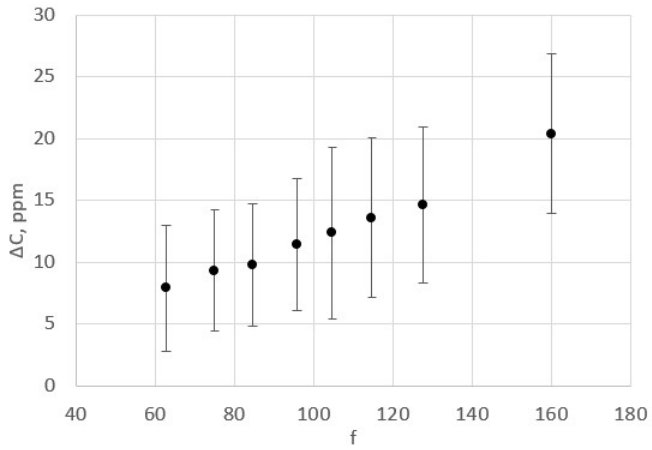

Fig. 4 Dependence of the average carbon increase at ACV ΔC from the carburization function f, for 2018-2020 years data for various IETS brands

Subsequent linear regression analysis between the carburization function and carbon gain showed that the probability of the null hypothesis of insignificance of the regression model is $1.94E-13$. The analysis involved grades of type $3Si-1Al, 3Si-0.5Al, 1Si-1Al$. The correlation plot, as well as the regression model with 95% confidence interval, are shown in Figure 3. Figure 4 shows similar data with the averaging of the ΔC value in the interval $\Delta f = 50$ with standard deviation.

Factor f has been calculated for all heats for last three years. Intervals with step $\Delta f = 50$ have been considered. Also, mean value of carbon pick-up has been calculated for heats, f factor of which belongs to specified intervals. Figure 3 shows positive monotonic dependence of the average carbon pick-up on f factor.

To get a more detailed estimation of a carbon pick-up trend, a number of extra probes have been taken during the consistent injection of ferrosilicon and aluminum and additives mixing till the end of RH pro-

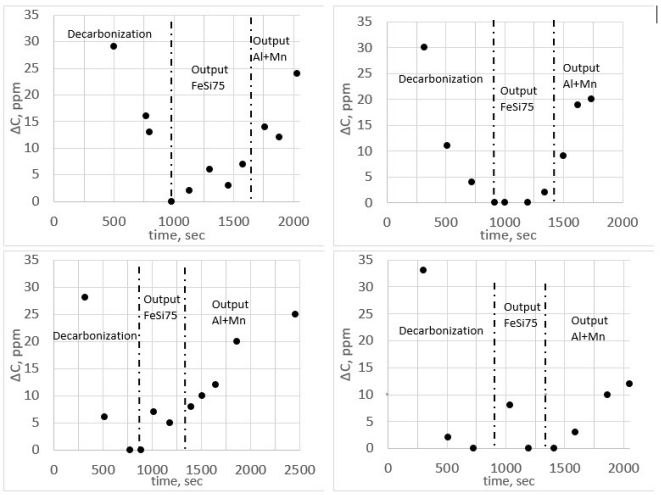

Fig. 5 Dynamics of carbon growth in the process of decarburization and mixing of alloying additives

cessing. A typical carbon pick-up trend is presented in Figure 5 for four different melts. The final probe of the de-carburization period is set as the baseline for evaluating the carbon increment ΔC. The dashed line splits the silicon and aluminum alloying periods. Based on studying of 18 heats the carbon pick-up for periods of FeSi and Al injections are estimated as ΔC_{FeSi} = 7±3 ppm and ΔC_{Al} = 10±5 ppm respectively. For both periods, carbon increment is a monotonic rising function without plateau which confirms the trend observed by many authors in laboratory conditions, as well as adopted in equation [1]. It is seen that the studied melts have different rates of carburization, which is probably due to the different chemical composition of the slag.

Thus for reduction of carbon increment one needs to reduce alloying amount or decrease time period or speed of mixing. The second scenario was chosen for further study, since the first leads to a significant deterioration in the properties of the product. As a result, a corrected mixing time should be proposed, which should be long enough to obtain a uniform distribution of alloying additions. In this paper, the authors chose numerical simulation as a tool to determine the optimal mixing time.

3 Mathematical Model and Methodology

The goal of the mathematical model is the determination of the local distribution of alloying additives in the volume of the ladle and degasser for stationary operation with a constant circulation rate (molten rate in the nozzles of the degasser) over time. From these re-

sults the total mixing time of the alloying additives is obtained, which is the target parameter of the model.

3.1 Assumptions

In this work, one phase turbulence model with governing continuity and momentum equations were used. The model for fluid flow in RH degasser is represented with the following assumptions:

(a) The fluid is considered viscous, incompressible and Newtonian [5,7,26,27,31? ,36]
(b) The fluid flow is a steady-state [5,7,25,27,29]
(c) The model is solved in the isothermal conditions because the heat transfer between argon gas and liquid happens right at the nozzle [5,7,26,27,30,36]
(d) Gravity force is not considered in the model
(e) Argon gas bubbles are not considered.
(f) Free surfaces in the vacuum chamber and in the ladle are assumed to be flat [5,7,20,26,27,29]
(g) The processes of the alloying additives injections, their melting as well as convection processes that they induce are neglected [5]
(h) The slag presence on the top surface of the liquid is neglected [5,20,25,26,27,30,31,36]

3.2 Governing Equations

Transport fluid has the density of 6300 kg/m^3, the kinematic viscosity of 9.30E-07 m^2/s, and the dynamic viscosity is 5.86E-03 Pa*s. With the assumptions considered above, the governing equations for the model are:

1. Continuity equation

$$\frac{\partial \rho}{\partial t} + \frac{\partial}{\partial x_j}(\rho u_j) = 0 \quad [2]$$

2. Momentum equation

$$\frac{\partial (\rho u_i)}{\partial t} + \frac{\partial}{\partial x_j}(\rho u_j u_i - \tau_{ij}) = -\frac{\partial p}{\partial x_i} + S \quad [3]$$

Where τ_{ij} is the shear stress tensor that can be expressed as

$$\tau_{ij} = (\mu + \mu_t)\left(\frac{\partial u_i}{\partial x_j} + \frac{\partial u_j}{\partial x_i}\right) - \frac{2}{3}\left((\mu + \mu_t)\frac{\partial u_k}{\partial x_k} + \rho k\right)\delta_{ij} \quad [4]$$

Variables used in the equations above are as follows: ρ – density; p - pressure; μ – dynamic viscosity; μ_t – turbulent viscosity; τ_{ij} – shear stress tensor; S – source term; u – velocity in the x, y, z coordinate projection; k – kinetic energy or turbulent pulsation, δ_{ij} – Kronecker delta.

For the turbulence, $k - \epsilon$ model is used, and it is based on the following equations:

- Dynamic viscosity expressed by Kolmogorov equation

$$\mu_t = \rho C_\mu \frac{k^2}{\varepsilon} \quad [5]$$

- Turbulent kinetic energy equation

$$\frac{\partial}{\partial t}(\rho k) + \frac{\partial}{\partial x_j}\left[\rho u_j k - \left(\mu + \frac{\mu_i}{\sigma_k}\right)\frac{\partial k}{\partial x_j}\right] = \mu_t (P + P_B) - \rho\varepsilon - \frac{2}{3}\left(\mu_t \frac{\partial u_i}{\partial x_i} + \rho k\right)\frac{\partial u_i}{\partial x_i} \quad [6]$$

- Turbulent dissipation rate equation

$$\frac{\partial}{\partial t}(\rho\varepsilon) + \frac{\partial}{\partial x_j}\left[\rho u_j \varepsilon - \left(\mu + \frac{\mu_t}{\sigma_\varepsilon}\right)\frac{\partial \varepsilon}{\partial x_j}\right] = \rho C_1 S\varepsilon - \rho C_2 \frac{\varepsilon^2}{k + \sqrt{v\varepsilon}} + C_{z3}\frac{\varepsilon}{k}\mu_t P_B + C_{\varepsilon 4}\rho\varepsilon\frac{\partial u_t}{\partial x_i} \quad [7]$$

- Turbulence generation due to normal and shear stresses

$$P = S_{ij}\frac{\partial u_i}{\partial x_j} \quad [8]$$

- Buoyancy effect term

$$P_B = -\frac{g_i}{\mathrm{Pr}_t}\frac{1}{\rho}\frac{\partial \rho}{\partial x_i} \quad [9]$$

- The mean strain rate

$$S_{ij} = \frac{1}{2}\left(\frac{\partial u_i}{\partial x_j} + \frac{\partial u_j}{\partial x_i}\right) \quad [10]$$

3.3 Boundary Conditions

At the refractory wall no-slip condition was applied, where r is the radius of the domain.

$$u_j(\vec{r}) = 0 \quad [11]$$

At the free surface in the chamber "slip wall" condition was used

$$\tau_{ij}(\vec{r}) = 0, u_n(\vec{r}) = 0 \quad [12]$$

Fluid circulation is set with two sources that are applied simultaneously. First, by applying the source term S_{val} in the up snorkel by means of the source term in the momentum equation. The source term S is parametrized to set the circulation rate. Below is the equation for the

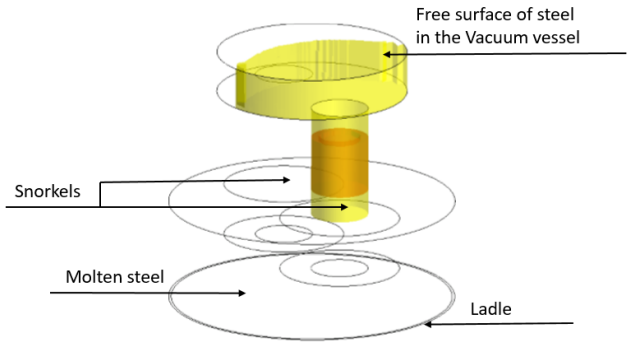

Fig. 6 Area for source term application (orange) and density decrease (yellow)

source term, where r is the radius with respect to the center axis of the down snorkel.

$$S = \begin{cases} S_{\text{val}}\ , (r < 0.31m) \wedge (y > h_2) \wedge (y < h_2 + 0.5m) \\ 0, \qquad \text{otherwise} \end{cases} \tag{13}$$

The second source involves setting the density field, which imitates the density decrease due to the argon gas and stimulates the flow circulation. Below, in Figure 5, the area where the source term is applied (orange) and the density inhomogeneity (yellow) is shown. In addition to the "slip wall" condition on the free surface, the boundary condition for alloying additives injection was used:

$$G_a = \begin{cases} \frac{\iiint_\Omega \rho \mathrm{d}v}{\iint_{A_{fv}} 1 \mathrm{d}s \cdot T_{inj}} & t < T_{inj} \\ 0, & t \geq T_{inj} \end{cases} \tag{14}$$

The equation above represents mass flow rate over the area of additives injection as a funciton of the additives mass, injection area and time. Mass is expressed in terms of the density over the volume integral of the space domain (Ω) and T_{inj} is the alloying additives injection time (set to 120s, but can be varied). The equation is normalized so that after the time period of the additives injection, the average concentration in the domain is equal to 1. As a result, a model was developed that uniquely relates the described sources and the average speed in the nozzle. The user sets the velocity, and the applied algorithm translates it into the parameters of the two sources described above.

3.4 Solution Tools

The finite volume method was used to solve the governing equations of the model. The method was implemented in the Ansys CFX software. The deformable mesh was utilized to change the snorkel immersion depth.

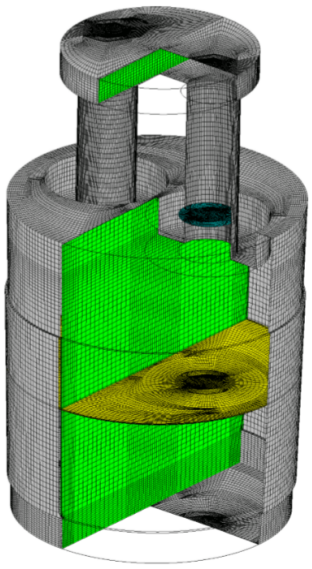

Fig. 7 Generated mesh for the volume studied is shown at different cross-sections

Boundary conditions and additional equations such as solution conditions and alloying additives injection are implemented by means of the CCL Ansys CFX programming language. Convergence criteria for the momentum and continuity equations are chosen to be 10^{-5} and for the turbulence equations 10^{-4}. Multi-block structures mash was chosen to get a good quality model that has a minimal number of volumes. To create the mesh for the model, Ansys ICEM-CFD tool was used. Mesh at different cross-sections is shown below in Figure 7. The mesh of the model presented has 1 184 832 nodes and 1 131 264 control volumes of total 24.0995 m^3.

4 Model Verification and Validation

The model created has many assumptions. Therefore it requires good validation and verification. Model validation was done by means of an industrial experiment. While model verification was made by means of checking the sensitivity of the mathematical model to various parameter changes using two solvers: Ansys CFX and STAR-CCM+.

4.1 Model Verification

The numerical model was solved in Ansys CFX and STAR-CCM+ with different parameters, to analyze the model response. The goal of the model verification was to prove that a simple model is reliable for obtaining results for the target parameter. The target parameter is the mixing time. The verification parameters in-

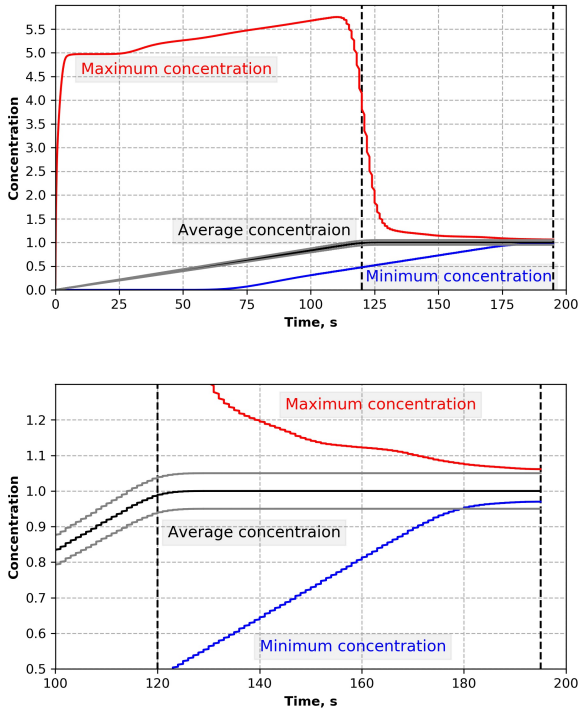

Fig. 8 Additives concentration (maximum, minimum and average) in the ladle for the 0.4 m SID and down snorkel velocity 1 m/s

clude the geometry complexity, mesh sensitivity, vacuum chamber free surface height, turbulence models and the area of the alloying additives injection. The variation all these parameters was done in both solvers, except the geometry simplification research, which was carried out only in STAR-CCM+ because it has better capabilities in terms of mesh generation for complicated geometries.

The typical profiles of the maximal and minimal aluminum additives concentration in the ladle are shown in Figure 8. The time when the average concentration level (black graph) reaches a saturation (the first vertical dashed line), is the end of the alloying additives injection and the start point of mixing time (the target parameter). Mixing time end point is when both maximum and minimum concentration values are within ±5% from the average concentration (the second vertical dashed line). It should be noted that regions of maximum and minimum concentrations are not placed in the fixed position inside the ladle. They migrate during the operational time. During the process of the model verification the effect of the geometry complexity, mesh sensitivity, vacuum chamber free surface height and the area of the alloying additives injection was studied. The results for all verification parameters except the turbulence models are displayed in Table 1.

One can observe that geometry complexity and additives injection area does not strongly affect the target parameter. However, the simplified geometry makes model computation cheaper, so it was used in the finalized model. Courser mesh is chosen, because it gives more conservative results and takes four times less computational time. The shorter time for the exaggerated height of the free surface might be affected by the velocity profile variation in the down snorkel. The regular height free surface approximation gives a conservative result, therefore the flat free surface assumption was used. Without such an assumption there would be intumescense of the surface above the up-leg snorkel, and velocity streamlines would have a high curvature in that area. Therefore, the choice of high level of free surface is an inverse extreme case of the stable free surface on the regular height, because the velocity streamlines are not curving due to the effect of interfacing with the free surface. It should be noted that all variation parameters presented in table 1 give no more than 13 % variation of target mixing time.

The turbulence models that were studied include quadratic and cubic $k-\epsilon$ realizable, and quadratic $k-\omega$ SST that were explored in STAR-CCM+. Along with SAT-SST (non-steady state), $k-\omega$, $k-\omega$-SST, $k-\epsilon$-RNG (non-steady state) and k-e models studied in Ansys CFX software. Results have shown that using the k-e model, described above, is a reliable and conservative choice.

4.2 Plant Experiment Methodology

Additive distribution, which was gained as a result of the simulation, was compared with the aluminum amount, measured during and right after dropping off aluminum granules during the high silicon electrical steel processing. Samples were taken from the same location as the samples for carbon analysis described in motivation section of this paper. Aluminum, as well as carbon, amount has been measured with optical emission spectrometer ARL ISPARK 8860. The evolution of aluminum concentration during aluminum discharge and mixing period is marked as dots in Figure 8. The values of discharge period, circulation rate and SID corresponds to operational values over the calculation. Results of the simulation on the top surface of the ladle and experimental probes from the location shown in Figure 2 are presented in figure 9. As one could observe, the agreement between the measured and calculated aluminum growth is satisfactory. Based on these data authors made a conclusion about the model validation.

Table 1 Verification parameters results

Parameter	Condition	Time when concentration is ±5% of average	Variation percent	Total mixing time
Geometry complexity	Simplified	320	3%	200
	Regular	310		190
Mesh sebsitivity	Global mesh size - 0.1 m	320	13%	200
	Global mesh size - 0.05 m	280		160
Free surface heigh	Regular height	320	13%	200
	Exaggerated height	280		160
Additives injection area	Full free surface area	320	0%	200
	30% of the free surface area	320		200

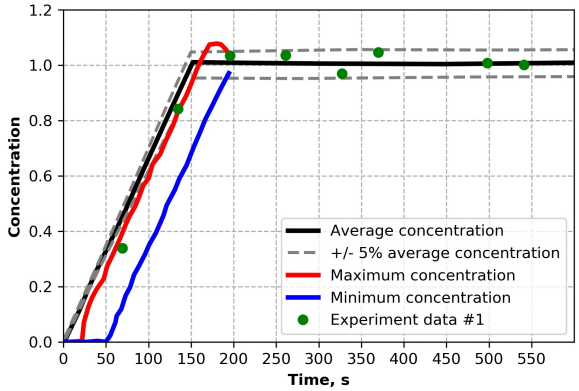

Fig. 9 Evolution of aluminum concentration on top of a ladle

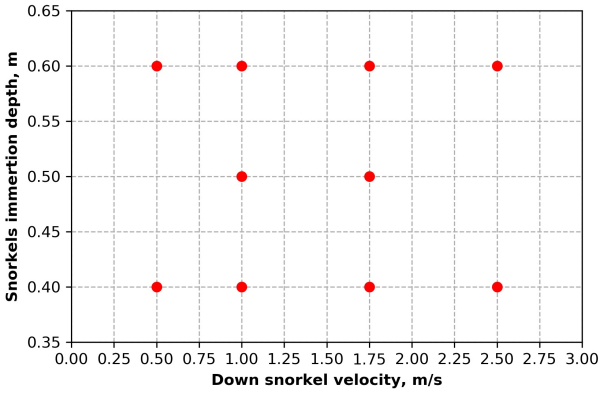

Fig. 10 Mode map

5 Results

The mathematical model had two variable parameters: snorkel immersion depth (SID) and velocity in the down snorkel. The regime map is shown below in Figure 10.

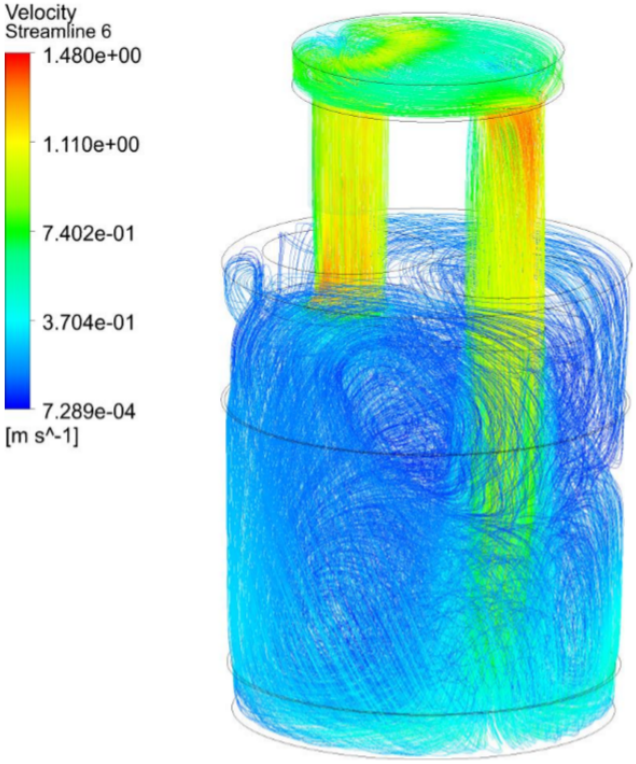

Fig. 11 Velocity streamlines representation for the 0.4 m SID and down snorkel velocity 1 m/s

The velocity streamlines, demonstrated below in figure 11, were obtained at the 0.4 m SID and velocity of 1 m/s. One can observe that the greatest velocity is in the snorkels, which is an upward velocity due to the argon gas injection (in this model the density difference). In the down snorkel, there is the downward velocity due to the fluid flow. From the plot in figure 6, one observes that alloying additives injection ended at 120s and minimum and maximum values have reached ±5% zone at around 190s. The exact value of mixing time in this example is 74.7 seconds.

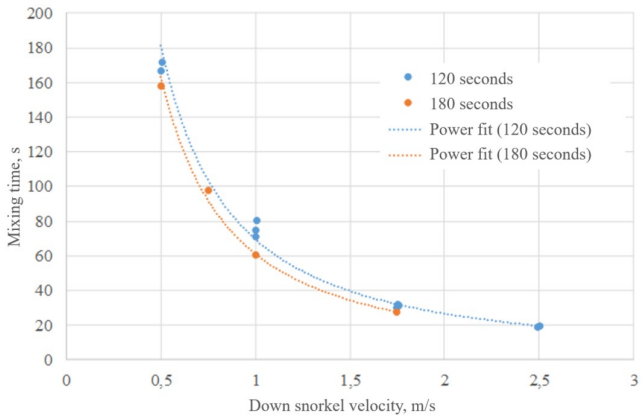

Fig. 12 Mixing time plot as a function of the down snorkel velocity for three SID values

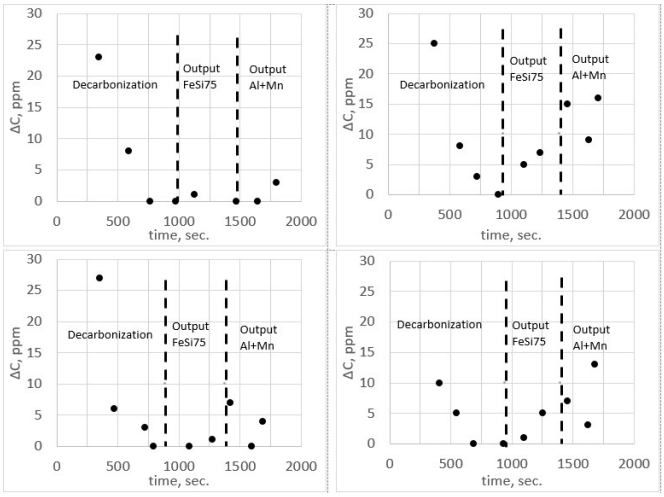

Fig. 13 Dynamics of carbon gain in the process of decarburization and mixing of alloying additives with the adjusted mixing technology

Similar model runs were performed for all the regimes shown on the regime map earlier. The results are summed up on the plot shown in figure 12. From the plot, one can observe that SID does not affect the mixing time as significantly as the down snorkel velocity does. For high velocities, SID does not have any effect. Mixing time dependence on the velocity is exponential and decreases with the velocity increase. For 0.4 m and 0.6 m SID experiments, the alloying additives injection time was 120s, while for the 0.5 m SID, injection time decreased up to 90s. From the plot, one can observe that decrease in the additives injection time by 30s increased the mixing time only by 10s. Decreasing the additives injection time might be an effective strategy, however, the additives injection time variation is not possible on the plant. Increasing of injection time up to 180 s keeping the same alloying amount reduces the mixing time for 10-20 s for all variation of circulation velocity.

The lowest possible circulation rate was chosen to minimize the carbon build-up during mixing on the evacuator. While the standard mixing mode implies mixing the additives at maximum circulation rates. The mixing time for the aluminum granules was determined for the selected speed in accordance with the dependence in Figure 12, taking into account the multiplication by a safety factor of 1.5-2. The mixing time for ferrosilicon was reduced slightly, since the existing equipment does not allow to reload the bunker with alloying additives faster.

As a result, carbon gain was analyzed for 12 heats with reduced stirring times. It was found that the increase in carbon after adding and mixing aluminum is no more than 6 ppm, which halved the increase in carbon at this operation. The dynamics of the increase in carbon with reduced stirring for four typical melts is shown in Figure 13. Similarly to the data in Figure 5, the carbon level at the time of the end of decarburization is taken as $\Delta C = 0$

Chemical analysis of hot rolled steel at various locations confirmed the homogeneous distribution of silicon and aluminum. Also, the absence of an increase in oxides in the slab was confirmed when the technology was adjusted.

6 Summary

In many works devoted to the study of the degradation of MgO-C refractories under the influence of interaction with slag and metal, it is indicated that the corrosion process develops over time according to a monotonically increasing law. Simultaneously with the destruction of the refractory matrix, carbon enters the melt. This effect of carburization is observed during processing on an RH-vacuum in the production of dynamo steels, which reduces the magnetic properties of the finished product.

A statistical analysis of production data for 3 years, as well as a detailed study of some heats, confirmed that carburization during the recoil and mixing process of alloying additives in a vacuum degasser has a monotonically increasing, close to a linear, dependence from time. The rate of carburization in heats is not constant and probably depends on the chemical composition of the slag and the condition of the ladle refractory. This issue should be investigated in subsequent works.

The authors proposed to reduce the mixing time of alloying additives to shorten the period with intense refraction corrosion and metal carburization. The problem of determining the time period sufficient for the

homogenization of the melt in the ladle was solved using computer simulation. A CFD model of the circulating evacuation process was developed, verified and validated, which makes it possible to estimate the mixing time required to homogenize the chemical composition. Numerical analysis was carried out for various combinations of nozzle immersion depth and circulation rate and a map of modes was built that can be applied to existing equipment. It was found that the rate of release of the additive and varying the depth of immersion of the nozzles in the selected ranges do not significantly affect the mixing time. Basically, the mixing time is determined only by the circulation rate, which in turn is controlled by the flow rate of the Ar lift gas. As a result, by means of CFD analysis, the optimal time required for chemical homogenization of the melt under various operating parameters was calculated.

According to the results of industrial testing of the calculated combinations of the circulation rate and mixing time on the existing vacuum apparatus, a decrease in the carbon gain to a level of < 6 ppm was obtained at the stage of Al recovery instead of < 15 ppm with was observed during the standard mixing. According to the analysis of hot rolled coils, the chemical homogeneity of the product is maintained when the technology is adjusted.

Therefore, it was shown on the example of the silicon electrical steel industrial production that one can reduce the carbon increase during the alloying additives mixing period in RH degasser without the decrease of the quality of the end product.

7 Nomenclature

Al – Aluminum concentration measured after t_{al} (ppm)
Si – Ferrosilicon concentration measured after t_{si} (ppm)
t_{al} – duration of mixing of Al (s)
t_{si} – duration of mixing of Si (s)
fut – number of heats for a ladle after the last repair
ρ – Fluid density (kg/m^3)
u – Velocity (m/s)
p – Pressure (Pa)
T_{ij} – Shear stress (Pa)
μ - Dynamic viscosity (Pa s)
μ_t – Turbulent viscosity (Pa s)
S – Source term (N/m^3)
k – Turbulent kinetic energy (m^2/s^2)
ϵ – Turbulent energy dissipation rate (m^2/s^3)
P_B – Production of turbulence due to particle drag (kg/ms^3)
P – Production of turbulence due to normal and shear stresses (kg/ms^3)
S_{ij} – Mean strain rate (1/s)
g – Gravity constant (m/s^2)
P_{rt} – Prandtl number
r - radial coordinate (m)
S_{val} – Source term (N/m^3)
T_{inj} – Alloying additives injection time (s)

References

1. P. Chanda, S. Sinha, S. Suresh, S.Kr. Singh, V.V.Mahashabde and A. Khullar: Production of ultralow-carbon steel by improving process control at RH degasser. AISTech - Iron Steel Technol. Conf. Proc. 2, 1491–1499 (2017)
2. S. He, G. Zhang and Q. Wang: Desulphurisation process in RH degasser for soft-killed ultralow-carbon electrical steels. ISIJ Int. 52, 977–983 (2012)
3. C. Schrade, H. Nicolai and Z. Zulhan: Desulfurization of Molten Steel in RH-Degasser by Powder Blowing to Produce Silicon Steel – Operational Results Maanshan ISCO Kinetic Model of Desulfurization by Powder Blowing. 15–19 (1891)
4. J. Zhang, Y. He, J. Liu, B. Yan, S. Zhang and W. Li: The effects of Soluble Gas Floatation Technology on the flow field of ladle and inclusion removal in RH refine process. Vacuum 168, (2019)
5. D.Q. Geng, J.X. Zheng, K. Wang, P. Wang, R. Liang, H. Liu, H. Lei, and J.C. He: Simulation on Decarburization and In*
6. V. Presen: Recent trends and the future of vacuum in steel making. Vacuum 43, 373–379 (1992)
7. G. Chen and S. He: Mixing behavior in the RH degasser with bottom gas injection. Vacuum 130, 48–55 (2016).
8. S.A. Nightingale, B.J. Monaghan and G.A. Brooks: Degradation of MgO refractory in CaO-SiO2-MgO-FeO x and CaO-SiO2-Al2O3-MgO-FeO x slags under forced convection. Metall and Materi Trans B 36, 453–461 (2005).
9. Y. J. Kim and D.J Min: Effect of FeO and Al2O3 on the MgO Solubility in CaO-SiO2-FeO-Al2O3-MgO Slag System at 1823 K. steel research int. 83, 852–860 (2012).
10. J.D. Shim and S. Ban-Ya: The Solubility of Magnesia and Ferric-Ferrous Equilibrium in liquid FeO-SiO2-CaO-MgO slags.pdf. Tetsu-to-Hagane 67(10), 1735–1744 (1981).
11. J.D. Shim and S. Ban-Ya: The Solubility of Magnesia and Ferric-Ferrous Equilibrium in liquid FeO-SiO2-CaO-MgO slags.pdf. Tetsu-to-Hagane 67(10), 1735–1744 (1981).
12. F. Huang, C. Liu, N. Maruoka, and S. Y. Kitamura: Dissolution behaviour of MgO based refractories in

CaO–Al_2O_3–SiO_2 slag. Ironmaking and Steelmaking 42, 553–560 (2015).
13. S. Jansson, V. Brabie, and P. Jonsson: Corrosion mechanism and kinetic behaviour of MgO-C refractory material in contact with CaO-Al2O3-SiO2-MgO slag. Scand J Metallurgy 34, 283–292 (2005).
14. M. K. Cho, M. A. Van Ende, T. H. Eun, and I. H. Jung: Investigation of slag-refractory interactions for the Ruhrstahl Heraeus (RH) vacuum degassing process in steelmaking. Journal of the European Ceramic Society 32, 1503–1517 (2012).
15. L. Chen, A. Malfliet, P. T. Jones, B. Blanpain, and M. Guo: Comparison of the chemical corrosion resistance of magnesia-based refractories by stainless steelmaking slags under vacuum conditions. Ceramics International 42, 743–751 (2016).
16. Y. Wei, Y. Dong, T. Zhang, J. Chen, and W. Yan: Influence of reaction of Al2O3 and carbonaceous materials in Al2O3–C refractories on aluminum and carbon pick-up of iron. J. Iron Steel Res. Int. 27, 55–61 (2020)
17. J. Poirier: A review: Influence of refractories on steel quality. Metall. Res. Technol. 112, (2015)
18. Y. Liu, L. Wang, G. Li, Z. Zhang, X. Xu, Y. Li, and J. Chen Effect of submicron-carbon-containing MgO-C refractories on carbon pickup of ultra-low carbon steel. J. Ceram. Sci. Technol. 9, 141–148 (2018)
19. F. Ahrenhold and W. Pluschkell: Mixing phenomena inside the ladle during RH decarburization of steel melts. Steel Res. 70, 314–318 (1999)
20. S.K. Ajmani, S.K. Dash, S. Chandra, and C. Bhanu: Mixing evaluation in the RH process using mathematical modelling. ISIJ Int. 44, 82–90 (2004)
21. S. Fan, B. Li, and J. He: Modeling of circulating flow in rh degassing vessel water model designed for two-and multi-leg operations. Jinshu Xuebao/Acta Metall. Sin. 37, 1100–1106 (2001)
22. Y.G. Park, K.W. Yi, and S.B. Ahn: The effect of operating parameters and dimensions of the RH system on melt circulation using numerical calculations. ISIJ Int. 41, 403–409 (2001)
23. Y.G. Park, W.C. Doo, K.W. Yi, and S.B. An: Numerical calculation of circulation flow rate in the degassing Rheinstahl-Heraeus process. ISIJ Int. 40, 749–755 (2000)
24. R. Tsujino, J. Nakashima, M. Hirai, and I. Sawada: Numerical analysis of molten steel flow in ladle of rh process. ISIJ Int. 29, 589–595 (1989)
25. K. Shirabe and J. Szekely: A Mathematical Model of Fluid Flow and Inclusion Coalescence in the R-H Vacuum Degassing System. Transactions ISIJ, Vol.23, 465-474 (1983)
26. D.Q. Geng, H. Lei, and J.C. He: Numerical simulation of the multiphase flow in the Rheinsahl-Heraeus (RH) system. Metall. Mater. Trans. B Process Metall. Mater. Process. Sci. 41, 234–247 (2010)
27. D.Q. Geng, H. Lei, and J.C. He: Simulation on flow field and mixing phenomenon in RH degasser with ladle bottom blowing. Ironmak. Steelmak. 39, 431–438 (2012)
28. B. Li and F. Tsukihashi: Effect of rotating magnetic field on two-phase flow in RH vacuum degassing vessel. ISIJ Int. 45, 972–978 (2005)
29. J. H. Wei and H. T. H: Mathematical modelling of molten steel flow in a whole degasser during RH refining process. Ironmak. Steelmak. 32, 427–434 (2005)
30. B. Zhu, K. Chattopadhyay, X. Hu, B. Zhang, Q. Liu, and Z. Chen: Optimization of sampling location in the ladle during RH vacuum refining process. Vacuum 152, 30–39 (2018)
31. G. Chen, S. He, and Y. Li: Investigation of the Air-Argon-Steel-Slag Flow in an Industrial RH Reactor with VOF–DPM Coupled Model. Metall. Mater. Trans. B Process Metall. Mater. Process. Sci. 48, 2176–2186 (2017)
32. G. Chen and S. He: Circulation flow rate and decarburization in the RH degasser under low atmospheric pressure. Vacuum 153, 132–138 (2018)
33. H. Ling, F. Li, L. Zhang, and A.N. Conejo: Investigation on the Effect of Nozzle Number on the Recirculation Rate and Mixing Time in the RH Process Using VOF + DPM Model. Metall. Mater. Trans. B Process Metall. Mater. Process. Sci. 47, 1950–1961 (2016)
34. C. Liu, H. Duan, and L. Zhang: Modeling of the melting of aluminum particles during the rh refining process. Metals (Basel). 9, 12–14 (2019)
35. Y. Liu, M. Ersson, H. Liu, P. Jönsson, and Y. Gan: Comparison of Euler-Euler Approach and Euler–Lagrange Approach to Model Gas Injection in a Ladle. Steel Res. Int. 90, 1–13 (2019)
36. P. A. Kishan, and S. K. Dash: Prediction of circulation flow rate in the RH degasser using discrete phase particle modeling. ISIJ Int. 49, 495–504 (2009)
37. D.Q. Geng, H. Lei, and J.C. He: Effect of traveling magnetic field on flow, mixing, decarburization and inclusion removal during RH refining process. ISIJ Int. 52, 1036–1044 (2012)
38. X. Ai, Y. Bao, W. Jiang, J. Liu, P. Li, and T. Li: Periodic flow characteristics during RH vacuum circulation refining. Int. J. Miner. Metall. Mater. 17, 17–21 (2010)
39. D. Mukherjee, A.K. Shukla and D.G. Senk: Cold Model-Based Investigations to Study the Effects of Operational and Nonoperational Parameters on the

Ruhrstahl–Heraeus Degassing Process. Metall. Mater. Trans. B Process Metall. Mater. Process. Sci. 48, 763–771 (2017)
40. J. Pieprzyca, T. Merder, M. Saternus, and K. Michalek: Physical modelling of the steel flow in RH apparatus. Archives of Metallurgy and Materials 60 (2015).
41. V. Seshadri, C.A. Silva, and I.A. Da Silva. Physical modeling simulations of refining processes in Brazilian Steel Industry. 340–352 (2005)
42. K. Zhang, H. Cui, R. Wang, and Y. Liu: Mixing phenomenon and flow field in ladle of RH process. Metals (Basel). 9, 1–12 (2019)
43. H. Ling, C. Guo, A.N. Conejo, F. Li, and L. Zhang: Effect of snorkel shape and number of nozzles on mixing phenomena in the RH process by physical modeling. Metall. Res. Technol. 114, (2017)
44. L. Lin, Y. Bao, F. Yue, L. Zhang, and H. Ou: Physical model of fluid flow characteristics in RH-TOP vacuum refining process. Int. J. Miner. Metall. Mater. 19, 483–489 (2012)
45. L. Neves, H.P.O. de Oliveira, and R.P. Tavares: Evaluation of the Effects of Gas Injection in the Vaccum Chamber of a RH Degasser on Melt Circulation and Decarburization Rates. 49, 1141–1149 (2009)
46. J. H. Wei: Physical modeling of the vacuum circulation refining process of molten steel. J. Shanghai Univ. 7, 1–17 (2003)
47. L. Zhang and F.E.I. Li: Investigation on the Fluid Flow and Mixing Phenomena in a Ruhrstahl-Heraeus (RH) Steel Degasser Using Physical Modeling. (2014)
48. J. Han, X. Wang, and D. Ba: Coordinated analysis of multiple factors of argon blowing parameters on the effect of circulation flow rate in RH vacuum refining process. Vacuum 109, 68–73 (2014
49. D.L. Niu, Q.C. Liu, D.R.Ma, J. Yang, M.R. Xu, and Z. Wang: Characteristics of the dead zones in RH desgasser with simulation methods. Mater. Sci. Forum 817, 755–763 (2015
50. T. Kuwabara, K. Umezawa, K.Mori, and H. Watanabe: Investigation of Decarburization Behavior in Rh-Reactor and Its Operation Improvement. Trans. Iron Steel Inst. Japan 28, 305–314 (1988)